

# Global Prediction of COVID-19 Variant Emergence Using Dynamics-Informed Graph Neural Networks

Majd Al Aawar

Ming Hsieh Department of ECE  
University of Southern California, USA  
malaawar@usc.edu

Srikanth Mutnuri

Ming Hsieh Department of ECE  
University of Southern California, USA  
mutnuri@usc.edu

Mansoor Montazerin

Ming Hsieh Department of ECE  
University of Southern California, USA  
mmontaze@usc.edu

Ajitesh Srivastava

Ming Hsieh Department of ECE  
University of Southern California, USA  
ajiteshs@usc.edu

**Abstract**—During the COVID-19 pandemic, a major driver of new surges has been the emergence of new variants. When a new variant emerges in one or more countries, other nations monitor its spread in preparation for its potential arrival. The impact of the variant and the timing of epidemic peaks in a country highly depend on when the variant arrives. The current methods for predicting the spread of new variants rely on statistical modeling, however, these methods work only when the new variant has already arrived in the region of interest and has a significant prevalence. The question arises: Can we predict when (and if) a variant that exists elsewhere will arrive in a given country and reach a certain prevalence? We propose a variant-dynamics-informed Graph Neural Network (GNN) approach. First, We derive the dynamics of variant prevalence across pairs of regions (countries) that applies to a large class of epidemic models. The dynamics suggest that ratios of variant proportions lead to simpler patterns. Therefore, we use ratios of variant proportions along with some parameters estimated from the dynamics as features in a GNN. We develop a benchmarking tool to evaluate variant emergence prediction over 87 countries and 36 variants. We leverage this tool to compare our GNN-based approach against our dynamics-only model and a number of machine learning models. Results show that the proposed dynamics-informed GNN method retrospectively outperforms all the baselines, including the currently pervasive framework of Physics-Informed Neural Networks (PINNs) that incorporates the dynamics in the loss function.

**Index Terms**—Graph Neural Networks, COVID-19 Variants, Forecasting

## I. INTRODUCTION

The COVID-19 pandemic presented an unprecedented global health crisis, severely affecting millions of people worldwide and demanding swift and effective responses from governments and healthcare providers [1]. As the pandemic progressed, multiple variants of COVID-19 emerged, each possessing unique genetic mutations that can significantly impact transmissibility, virulence, and even vaccine efficacy. During much of the COVID-19 epidemic, the surge in cases and severe outcomes (hospitalizations and deaths) have been driven by the emergence of new variants [2]. Consequently, monitoring the emergence and spread of these variants is crucial for devising appropriate public health measures and

optimizing containment strategies [3]. A critical factor driving the surge in a given region is the time of arrival of the new variant [4]. We can observe how a new variant, that has not appeared in region  $A$  yet, spreads in region  $B$ . We can study the spread in the region  $B$  to understand the properties of this new variant. If it is a highly transmissible or immune-evading variant [5], we can expect it to spread in the region  $A$  eventually. However, when it happens in region  $A$  precisely remains unknown. Therefore, making a good prediction of arrival time would lead to a more effective preparation and resource management.

In this paper, we focus on the problem of predicting arrival of a new variant in a given region provided that it has appeared somewhere else. This can be posed as a set of two problems: (1) A new variant  $X$  has arrived and is spreading in region  $A_1, A_2, \dots$ , but not yet in region  $B$ . Will it arrive in region  $B$ ? (2) If yes, when will it arrive in region  $B$ ? Since there may be some false positives and noise in the data, a variant may seem to have appeared but not spreading. Furthermore, a variant may start to spread, but quickly get dominated by another variant before it reaches a significant proportion of the circulating cases. This can be seen in Figure 1, which shows the proportions of a few different variants in the UK and Sweden. Therefore, we reformulate the two problems as the following:

**Problem 1** (Emergence Prediction). *Given the prevalence (proportion) of a variant in regions  $A_1, A_2, \dots$ , predict if the variant will ever reach a proportion  $\theta$  (we say, dominance threshold) in region  $B$ .*

**Problem 2** (Delay Prediction). *Given the prevalence (proportion) of a variant in regions  $A_1, A_2, \dots$ , predict when the variant will reach a proportion of  $\theta$  in region  $B$ .*

Here, the term “proportion” refers to the fraction of cases created by the variant under consideration of the total cases.

It naturally follows from the above description that *Problem 1* is a classification problem while *Problem 2* is a regression problem. In practical scenarios, we envision addressing *Prob-*

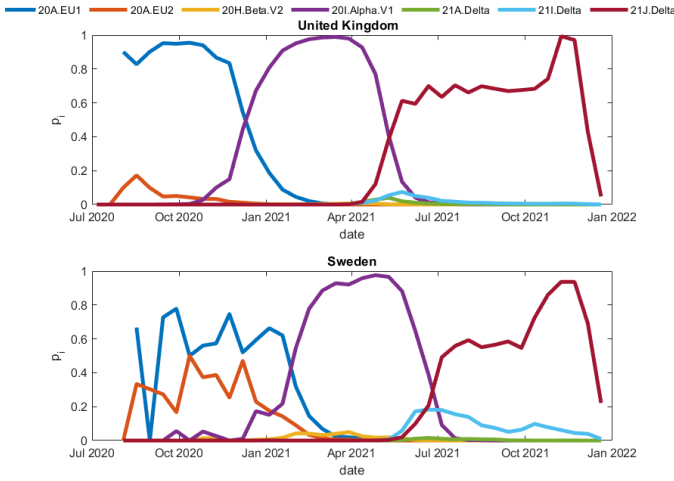


Fig. 1: Plots showing the prevalence of a few different variants of COVID-19 over time in the UK and Sweden. The beginning of the spread of new variants can differ across countries by several weeks. This can be seen when examining the “20I.Alpha.V1” and “21J.Delta” variants in the provided plots, which show their appearance in the UK several weeks before reaching Sweden.

*lem 1* first, and only tackling *Problem 2* if the outcome is positive. This is also important for the sake of evaluation as we can answer *Problem 2* only if the variant actually arrives in the region of interest. Existing work has focused on the problem of predicting the prevalence of a variant when it has already arrived in the region of interest [6]–[8]. Specifically, logistic regression turns out to provide a good estimate of the prevalence over time [9], [10]. However, these techniques require the variant to have a non-zero proportion already in the region of interest. To the best of our knowledge, no prior work exists predicting the delay to reach a certain prevalence even when there is zero prevalence in the region. We show that *Problem 1* (Emergence prediction) is a simpler problem (albeit, non-trivial) that can be solved by a decision tree. However, *Problem 2* (delay detection) is more difficult to solve and requires more sophisticated techniques.

When a new variant emerges with evolutionary favorable properties, the only way it can be transferred to a different region is through a host (human). This encourages the idea of using an underlying network of mobility to address the proposed problems. Since reaching a certain prevalence may depend on the other currently circulating variants, their dynamics (how fast one variant can spread over others) also play a role. Therefore, we propose a variant dynamics-informed Graph Neural Network (GNN) that utilizes a network of mobility and features inspired by variant dynamics to solve the proposed problems. This is different than typical Physics-Informed Neural Networks (PINNs) where the dynamics act as a regularization for the loss [11]. Here, we show that our approach of constructing appropriate features results in lower errors than incorporating the dynamics in the loss function.

Our key contributions represent a novel effort in addressing the challenge of predicting the emergence of COVID-19 variants at a global level, and in doing so establishing a new benchmark for evaluating Emergence Detection and Delay Prediction on the CoVariants dataset [12]. More specifically, our contributions are as follows:

- 1) We derive the variant dynamics, under some assumptions, that leads to a model of the delay for a variant reaching a certain prevalence between a pair of countries. This model serves as a baseline in our exploration, providing valuable insights that can be leveraged by our GNN and other Machine Learning (ML) models.
- 2) We develop novel adaptations of GNNs which incorporate disease dynamics into the models. This innovative approach significantly improves the predictive performance, by accounting for the complex inter-dependencies between countries. Through some experiments, we demonstrate that our approach leads to superior results compared to several ML methods, including the currently pervasive framework of PINNs that include the dynamics in the loss function.
- 3) We make our evaluation pipeline publicly available <sup>1</sup> so that it can be used by any user-defined PyTorch model for evaluation, thus providing a new benchmark for the community.

## II. RELATED WORK AND BACKGROUND

### A. Variants and Variant Dynamics

In the context of infectious diseases, the term “variant” refers to a version of a virus with some changes in its genetic material, known as genome [13]. These changes happen through genetic mutations and can affect the virus’s characteristics, like how easily it spreads, how severe the illness it causes is, and whether it can evade the immune system or not. Variants can be categorized in multiple ways based on genetic differences, and the significance of these differences can vary. Some categorizations focus on a common ancestor, while others may specifically highlight mutations in key regions of the virus’s genome [13]. In our study, we rely on the categorizations provided by the CoVariants dataset, discussed further in Section IV-A.

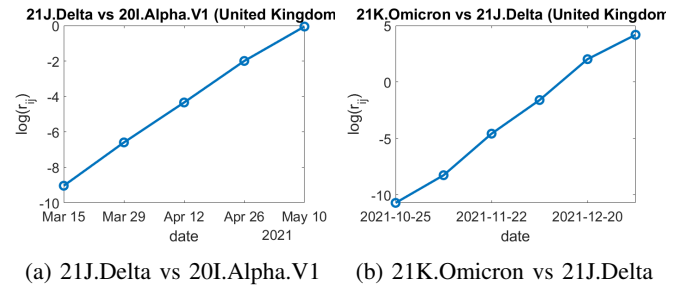


Fig. 2: Example semi-log plots of variant proportions from data in the CoVariants dataset.

<sup>1</sup>GitHub Link

Furthermore, it's worth noting that the proportions of different variants can be analyzed over time. Some studies have observed that these proportions follow a straight line when plotted on a semi-logarithmic scale. Therefore, they leverage this fact to understand the dynamics of variant emergence and prevalence in populations [14]. We also observe this in our data as shown in Figure 2. However, to the best of our knowledge, existing studies do not derive any dynamics capable of predicting delays in the emergence of variants between multiple regions/countries.

### B. Graph Neural Networks and Epidemics

In response to the COVID-19 pandemic, many efforts were made to develop forecasting models capable of predicting the progression and future trends of the COVID-19 pandemic [15]–[17]. However, these forecasting approaches have primarily focused on predicting overall case counts, hospitalizations, or mortality rates, rather than predicting delays in variant emergence. The ability to predict the timing of variant-specific outbreaks can significantly enhance public health preparedness and response strategies, allowing for timely interventions such as targeted vaccination campaigns and tailored public health measures [3].

Many Deep Learning (DL) techniques have been explored for predicting the dynamics of infectious diseases. While many models use methods like GNNs [18], and PINNs [19] for forecasting, some approaches have also focused on genetic sequence modeling for variants [20], [21].

E. Kharazmi et al. [22], use PINNs in epidemiological models to better capture the dynamics through the underlying Ordinary Differential Equations (ODEs). These works are normally variations of the classical Susceptible-Infectious-Removed (SIR) model with additional compartments [23]. Extending this, A. Rodríguez et al. [24] propose a framework for forecasting, Epidemiologically-informed Neural Networks (EINNs) that integrates epidemiological knowledge embedded in ODE models into neural networks. The core idea is utilizing the learned representations from a PINN using transfer learning along with a neural network that ingests multi-modal data. Other extensions include Epi-DNNs from X. Ning et al. [25], in which the neural network expresses the unknown parameters in the compartmental model, and the ODEs are solved using the Runge-Kutta method.

Since infectious diseases inherently present across multiple regions over a period of time, network models, like GNNs help in capturing the low-level graph effects. Works [26]–[30], including Gao et al. [27] rely on GNNs to predict the total number of cases for a fixed period in the future using a spatio-temporal attention network. These models typically map locations (e.g., a county or a state) to nodes on a graph and construct the edges based on geographical proximity and demographic similarity between locations. As an extension, [31], [32] combines spatio-temporal GNNs with PINNs. [33], [34] use agent-based models on top of these to further capture low-level interactions between populations in different compartments.

While some works do focus on using the spatio-temporal networks with location aware features [35], including mobility data [36], to the best of our knowledge, no studies have attempted to predict the emergence of a variant in one country based on its occurrence in another (*Problems 1 & 2*), through variant informed dynamics.

In summary, instead of predicting the spread of the virus (reported cases, deaths, and hospitalizations), as others have done, we aim to predict if and when a new variant will emerge in a region given that it has emerged elsewhere. This involves deriving the dynamics of variant spread and incorporating these insights into a GNN. Notably, our strategy revolves around crafting relevant features rather than altering the loss function, providing a distinctive and effective method for predicting variant emergence.

## III. METHODOLOGY

### A. Variant Dynamics

First, we develop an understanding of the dynamics that play a role in the spread of a new variant and how we can utilize them to make informed predictions. These dynamics can be epidemiological, spatial, or temporal. We start by extracting each variant's *global growth rates* (see Section III-B) from the data. This value provides an indication of the dominance of the variants over other competing ones. Next, we build a model based on the dynamics of infectious diseases and the derived growth rates. This model is used as a baseline for *delay prediction*. Finally, we consider different approaches in which we can incorporate some disease dynamics using GNNs that are chosen for their ability to intuitively model spatial dynamics, with the goal of enhancing the prediction accuracy of our model. Throughout the text, we use the terms "prevalence" and "prevalence ratio" as defined below:

$$\text{Prevalence}(p_i) = \frac{\# \text{ of COVID cases of a given variant } i}{\text{Total } \# \text{ of all cases}} \quad (1)$$

$$\text{Prevalence Ratio}(r_{ij}) = \frac{p_i}{p_j} \quad (2)$$

where  $p_i$  is the prevalence of the variant  $i$ , and  $p_j$  is the prevalence of the most prevalent variant,  $j$ , that is not  $i$ . For a variant to be considered dominant, it must reach an  $r_{ij}$  value of at least  $\frac{1}{3}$ . We define this value as the *dominance threshold*,  $\theta$ .

### B. Variant Growth Rates

We first derive the dynamics of two competing variants in one region. While logistic regression has been widely used to fit these dynamics, for completeness, we present a derivation. We start by using a model of infectious diseases that generalizes a large class of models [37]:

$$\begin{aligned} \Delta I(t) &\approx \beta \kappa(t) \bar{S}(t) \sum_{\tau=0}^{\infty} \bar{\alpha}(\tau) \Delta I(t - \tau) \\ &\approx \beta \bar{S}(t) \Delta I(t - b)(1 + \epsilon_t) \end{aligned} \quad (3)$$

where  $\Delta I(t)$  is the new infections at time  $t$ ,  $\bar{\alpha}(\tau)$  are transmission parameters,  $\bar{S}(t)$  is the fraction of susceptible population, and  $\epsilon_t$  is some small number. The number of contacts at time  $t$  is given by  $\kappa(t)$ . The approximation follows from Taylor expansion, and using the fact that  $\Delta I(t)$  is a smooth function. The constant  $b$  happens to be the mean serial interval – the average time between two successive infections. Now, given two variants  $i$  and  $j$ , assuming full cross-immunity between all variants, i.e.  $\bar{S}_i(t) = \bar{S}_j(t) = \bar{S}(t)$ , the prevalence ratio is approximated as:

$$\begin{aligned} r_{ij}(t) &= \frac{\Delta I_i(t)}{\Delta I_j(t)} \approx \frac{\beta_i \kappa(t) \bar{S}(t) \Delta I_i(t - b_i)}{\beta_j \kappa(t) \bar{S}(t) \Delta I_j(t - b_j)} \\ &\approx \frac{\beta_i \Delta I_i(t - b)}{\beta_j \Delta I_j(t - b)} = \beta_{ij} r_{ij}(t - b) \end{aligned} \quad (4)$$

The above further assumes that the mean serial intervals of the two variants are close, i.e.,  $b_i = b_j = b$ . Note that we assumed full cross-immunity which is true for a number of variants before the Omicron sub-variants [38]. If there is only a partial cross immunity,  $\bar{S}_i(t) \neq \bar{S}_j(t)$ . However, in a short interval, the new immunity (reduction in susceptibility) created by the variants is small. As a result, it can be shown that  $\bar{S}_i(t) \approx \beta'_{ij} \bar{S}_j(t)$  for some constant  $\beta'_{ij}$  which can be absorbed in the parameter  $\beta_{ij}$  above. Solving the above recurrence relation, we get:

$$r_{ij}(t) = (\beta_{ij})^{t/b} r_{ij}(0)$$

Taking the logarithm reduces the equation to:

$$\ln(r_{ij}(t)) = \frac{t}{b} \ln(\beta_{ij}) + \ln(r_{ij}(0)) = S_{ij}t + C \quad (5)$$

The parameter  $S_{ij}$  can be referred to as the relative growth rate of variant  $i$  over variant  $j$  [37]. Now, consider a scenario in two regions  $A$  and  $B$  —  $A$  has the variant  $i$  emerging over the previously dominant variant  $j$ ; but variant  $j$  never reached region  $B$  where variant  $k$  is dominant. This makes it difficult to assess the potential impact of variant  $i$  on region  $B$  when we only know  $S_{ij}$ . To deal with this challenge, we note that the parameter  $S_{ij}$  should ideally be independent of the region (this may not hold due to the simplifying assumptions above, so we actually have a **region-specific relative growth rate**  $S_{ij}^{(p)}$  for region  $p$ ). Therefore, we can attempt to find the growth-rate of any variant  $i$  with a fixed variant 0, specifically, the original COVID-19 variant. For ease of notation, we represent the growth advantage of variant  $i$  with respect variant 0 as  $S_i$ , with  $S_0 = 0$ , and refer to these values as **global growth rates**. Ideally,  $S_{ij} = S_i - S_j$ , irrespective of the region where the  $S_{ij}$  is estimated. To estimate these the global growth rates for all the variants that exist by the time  $t$  over all regions  $p$ , we can set up the following system of linear equations:

$$S_i - S_j = S_{ij}^{(p)} + \epsilon_{ijp}, \forall i, j, p, \quad (6)$$

where  $S_{ij}^{(p)}$  is the growth advantage of variant  $i$  over variant  $j$  in region  $p$  and  $\epsilon_{ijp}$  are error terms. The solution is given

by minimizing the sum of squares of  $\epsilon_{ijp}$ . We, then, define an objective function and solve for the  $S_i$  value as

$$\sum_{i,j,p} \epsilon_{ijp}^2. \quad (7)$$

Finally, based on the global growth rates, we define **global relative growth rates**  $S_{ij}$  as  $S_i - S_j$ .

These growth rates are used in our proposed methods for both *Emergence Prediction* and *Delay Prediction*. We note in our Benchmarking study, Section IV-E, that existing simple ML models with our constructed features produce very high accuracy for the former problem. Therefore, we focus on our approaches for the latter problem next.

### C. Dynamics-based Model

Consider three variants  $i$ ,  $j$ , and  $k$  where  $i$  is an emerging variant. We assume that either of the following holds – (i) Variants  $j$  and  $k$ , respectively in regions  $X$  and  $Y$ , are the variants that constitute most of the other infections; or (ii) All variants other than  $i$  in the respective regions  $X$  and  $Y$  have similar enough global growth rates that can be grouped into variants  $j$  and  $k$ . Suppose variant  $i$  appears in region  $X$  first, followed by region  $Y$ . Then we have:

$$\ln \left( \frac{p_i^Y(t)}{p_j^Y(t)} \right) = S_{ij}(t - t_0) + C'_Y \quad (8)$$

$$\ln \left( \frac{p_i^X(t)}{p_k^X(t)} \right) = S_{ik}(t - t_0) + C'_X \quad (9)$$

For a new variant, initially, the number of infections increase because of the new infections coming from a different region (importations). After some point, when transmission starts to happen within region (community transmission), the imported infections become negligible in comparison, and this is the point after which above equations are valid.

Suppose we select  $t_0$  as the time at which  $p_i^X(t_0)$  is large enough such that the community transmission dictates the dynamics in the region  $Y$  rather than importations and so, both Equations 8 & 9 hold for  $t \geq t_0$ . Suppose that the threshold for prevalence in region  $Y$  for community transmission to dominate is  $\theta_Y$  and that for region  $X$  is  $\theta_X$ . We assume that  $\theta_X$  and  $\theta_Y$  are independent of the variant. Then, by setting  $t = t_0$  in equations 8 & 9, we get:

$$\ln \left( \frac{\theta_Y}{1 - \theta_Y} \right) = C'_Y \quad \text{and} \quad \ln \left( \frac{\theta_X}{1 - \theta_X} \right) = C'_X \quad (10)$$

Therefore, both  $C'_Y$  &  $C'_X$  are variant independent. Let  $t_Y^\theta$  and  $t_X^\theta$  be the times at which variant  $i$  reach target prevalence of  $\theta$  in regions  $Y$  and  $X$ , respectively. We want to find  $\tau = t_Y^\theta - t_X^\theta$ . From equations 8 and 9:

$$\begin{aligned} \ln \left( \frac{\theta}{1 - \theta} \right) &= S_{ij}(t_Y^\theta - t_0) + C'_Y = S_{ik}(t_X^\theta - t_0) + C'_X \\ \implies S_{ij}\tau &= (S_{ij} - S_{ik})(t_X^\theta - t_0) + C'_X - C'_Y \end{aligned} \quad (11)$$

Also from equation 9:

$$t_X^\theta - t_0 = \frac{1}{S_{ik}} \left( \ln \left( \frac{\theta}{1-\theta} \right) - C'_X \right). \quad (12)$$

Plugging this value into equation 11, we get:

$$\begin{aligned} S_{ij}\tau &= \frac{(S_{ij} - S_{ik})}{S_{ik}} \left( \ln \left( \frac{\theta}{1-\theta} \right) - C'_X \right) + C'_X - C'_Y \\ \Rightarrow \tau &= \frac{S_{kj}}{S_{ij}S_{ik}} \ln \left( \frac{\theta}{1-\theta} \right) - \frac{S_{kj}}{S_{ij}S_{ik}} C'_X + \frac{C'_X - C'_Y}{S_{ij}} \end{aligned} \quad (13)$$

Here  $\theta$  is a given prevalence,  $S_{ij}$ ,  $S_{ik}$ , and  $S_{kj}$  are global relative growth rates estimated as shown in Section III-B.  $C'_X$  and  $C'_Y$  are unknowns. Therefore for each pair of regions  $X$  and  $Y$ , to identify the delay in reaching a given prevalence  $\theta$ , we can build a linear model  $Y = W^T Z$

$$\begin{aligned} Y &= \tau(i, j, k, \theta) - \frac{S_{kj}}{S_{ij}S_{ik}} \ln \left( \frac{\theta}{1-\theta} \right) \\ Z &= \begin{bmatrix} -\frac{S_{kj}}{S_{ij}S_{ik}} \\ \frac{1}{S_{ij}} \end{bmatrix} W = \begin{bmatrix} C'_X \\ C'_X - C'_Y \end{bmatrix} \end{aligned} \quad (14)$$

We then use the calculated weights from our linear models in equation 14 and plug them into equation 13 to find the  $\tau$  value between two regions. This is a pairwise model that estimates the delay between two regions rather than providing a delay from the current date. Algorithm 1 shows how we compute the date at which a variant arrives in a given region  $Y$ , we calculate the median of the outputs from all pairwise models from region  $X_p$  to region  $Y$ . We evaluate the performance of all the models ( $X_p, Y$ ) until the current date, and pick the top three source regions among  $\{X_1, X_2, \dots\}$ . The median of these selected models is then taken to represent the delay at time  $t$  for the new variant.

---

**Algorithm 1** Dynamics-based Arrival Date Computation

---

- 1: **for all**  $X_p$  in  $\{X_1, X_2, \dots\}_t$  **do**
  - 2:   Calculate and store delay predictions for  $(X_p, Y)$  until the current date,  $t$ .
  - 3: **if**  $t \neq 0$  **then**
  - 4:   Select top 3  $X_p$  with the best performance at  $t - 1$
  - 5: **else**
  - 6:   Select all source regions  $\{X_1, X_2, \dots\}_t$
  - 7: Find the median of delay predictions for selected models
  - 8: **return** Median delay as the estimated arrival date for the variant in region  $Y$  at time  $t$
- 

#### D. Dynamics-Informed GNN

We propose a GNN-based network for this problem as GNNs are adept at capturing spatial relationships, making them well-suited for problems where geographical proximity between regions, such as countries, plays a crucial role. Additionally, the problem induces a natural graph structure, where countries can be represented as nodes with edges denoting some relationship between the countries. Furthermore, we

explore different techniques to incorporate disease dynamics into the GNN in an effort to capture the complex interactions and patterns associated with the spread of infectious diseases.

1) *Graph Construction*: The graph construction is illustrated in Figure 3. First, we represent each country as a node in the graph and edges in the graph are established to represent relationships between the countries. There are a total of 87 countries in which at least one variant appears and becomes dominant in the CoVariants dataset [12]. While not shown in Figure 3, self-loops are included to account for internal transmissions. Next, we consider temporal aspect of the problem. The graph may evolve over time to capture changing relationships or influences among countries. This is introduced into our graph as dynamic edge weights based on border control data in the OxCGRT dataset [39]. Section IV-A provides more details on this dataset and its pre-processing.

To obtain the full graph, we create multiple copies of the above graph representing regions and inter-connectivity – one per variant. This approach allows us to leverage variant-specific dynamics as our node features. For each node  $c$ , the considered features consist a time series of the log of prevalence ratios  $r$  of a present variant  $i$  as defined in equation 2, for  $T$  time steps. This results in a vector  $r_{c,i}$  and the corresponding  $S_i$  value of this variant. These components are then concatenated to form each node's final feature vector  $[r_{c,i}|S_i]$ . The selection of these features was informed by our derivation in Equation 5, which shows that, under some assumptions, there exists a simple linear relation between the two. We hypothesize that these features simplify the underlying patterns that are then more easily learned by a GNN that may complement the violation of the assumption of the dynamics-based model.

2) *Temporal Encoded Graph Convolutional Network (T-GCN)*: In order to extract both temporal and geographical information of the data, we propose a hybrid architecture summarized in Figure 4. In this model, we employ a simple Gated Recurrent Unit (GRU) [40] to extract temporal information of the variant transmissions in  $T$  time steps. We temporarily remove the growth rate  $S_i$ , which is not time-dependent, from node features and embed the 1-dimensional (1D) time-dependent features (prevalence ratios) into a 2D latent feature vector. Note that in this configuration, we embed the features separately for each country, treating the nodes as distinct input samples grouped into a single batch, resulting in a 3D latent feature vector. The 3D latent feature vector is then flattened to obtain a final 2D embedding, which serves as input for a one-layer Graph Convolutional Network (GCN). The Leaky ReLU activation function introduces non-linearity after the GCN layer. Additionally, two GraphNorm [41] layers are applied after the GRU and GCN layers for normalization, and dropout is incorporated after the GCN layer for regularization. Finally, the embedded features are fed into a Fully Connected (FC) layer to predict delay and emergence for each country.

3) *Dynamics-Informed Loss GCN (DIL-GCN)*: In this approach, we explicitly guide our GCN, described in Section

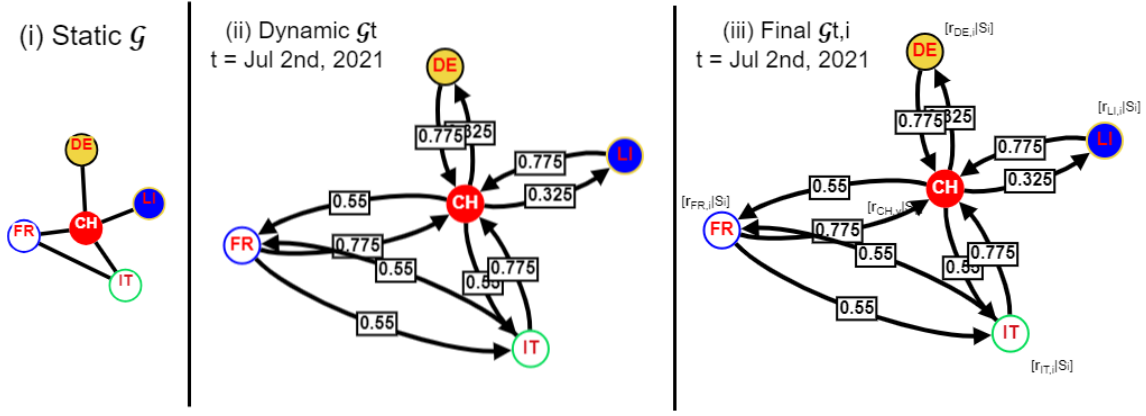


Fig. 3: Graph creation process on sample subgraph  $\mathcal{G}$ : (i) first we construct our nodes and edges based on country adjacency (ii) Next, we account for temporal variations in the relations between countries, i.e. the edges, to get a  $\mathcal{G}_t$  (iii) Finally, we find the variant specific features to get our sample graph  $\mathcal{G}_{t,i}$

IV-D, to make predictions based on dynamics, specifically for the delay prediction task. This guidance is achieved by incorporating information from our dynamics-based model. Given that our GCN is trained using a Mean Squared Error (MSE), the loss function is:

$$\text{MSE} = \frac{1}{N} \sum_{i=1}^N (\hat{y}_i - y_i)^2 \quad (15)$$

where  $N$  is the number of countries,  $\hat{y}_i$  is our models output, and  $y_i$  is the ground truth. We modify this loss function to steer our GCN towards dynamic predictions inspired by the dynamics-based model. This technique is typically used in PINNs [11]. The adjusted loss function is given by:

$$\text{MSE}_{\text{adjusted}} = \frac{1-p}{N} \sum_{i=1}^N (\hat{y}_i - y_i)^2 + \frac{p}{N} \sum_{i=1}^N (\hat{y}_i - \dot{y}_i)^2 \quad (16)$$

where  $p$  is a hyperparameter ranging from 0 to 1, signifying the influence of  $\dot{y}_i$ , the output from the dynamics-based model. This modification ensures that, during training, the model is penalized more when its prediction deviates from the linear model's prediction, providing a form of dynamics-informed regularization. The best  $p$  value was found to be 0.1 by validating on both logarithmic and linear ranges of  $p$ .

#### E. Training Procedure

All training and validation of the models were performed retrospectively, as outlined in Algorithm 2. This means that the model is trained and validated at each time step using only the "observed" data available up to that time step, denoted as  $d$ . For each variant, the algorithm iterates through all the biweekly data associated with that variant, training the model only on the weeks that have already passed (i.e., the observed data). It is important to note that the pre-processing is also done retrospectively, accounting for any smoothing, calculation of the  $S$  values, or interpolation in the case of the dynamics-based model. This ensures that the approach is

#### Algorithm 2 Retrospective Training and Validation

```

1: for variant in variants do
2:   dates  $\leftarrow$  unique dates in which variant exists
3:   model_initial_weights  $\leftarrow$  random
4:   for  $d$  in dates do
5:     retro_D  $\leftarrow$  all data before  $d$ 
6:     processed_D  $\leftarrow$  pre-process(retro_D)
7:     dataset  $\leftarrow$  structure processed_data into graphs
8:     train_D, val_D  $\leftarrow$  dataset split 80/20%
9:     model  $\leftarrow$  initialize with model_initial_weights
10:    epochs  $\leftarrow$  100
11:    early_St  $\leftarrow$  Early Stopper(patience=3)
12:    model.train(epochs, early_St, train_D, val_D)
13:    best_model_weights  $\leftarrow$  early_St
14:    model_initial_weights  $\leftarrow$  best_model_weights

```

applicable in a prospective setting, where no data from the future is available.

The train/validation split is done temporally to ensure that validation is performed only on the most recently observed data. This approach aims to achieve a better fit to the latest data, enhancing the model's predictive performance. An Early Stopper monitors the validation loss and halts the training when overfitting is detected, signified by a constant and significant increase in the validation loss. The Early Stopper saves the best-performing weights, which are then reused in the next iteration as a form of transfer learning. This practice eliminates the need for the model to start training from scratch, leveraging knowledge gained from previous iterations.

While Algorithm 2 shows the general approach taken for the training, problem-specific aspects are discussed below.

1) *Delay Prediction:* Since this is a regression task, we use MSE as the loss function (Equation 15). Another crucial aspect is how to handle data related to variants that either do not appear in a given country or appear but fail to become dominant, i.e. rapidly diminish. In such cases, where

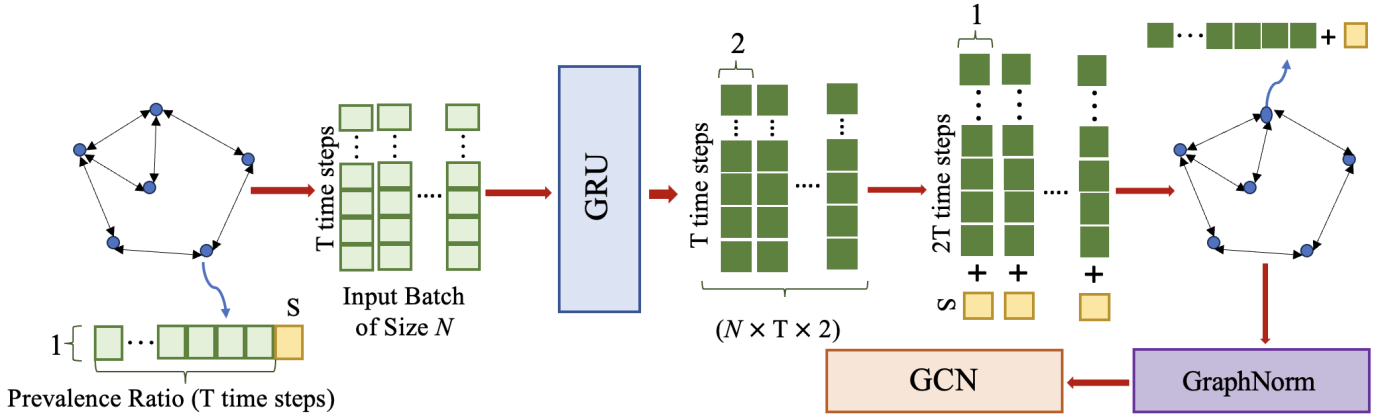


Fig. 4: T-GCN Architecture. The prevalence ratio for each time step is encoded into a 2D latent feature vector by the GRU. Then, the feature vectors are flattened and the growth rate is concatenated to them. Our batch size of  $N = \#$  of countries.

regression targets would be undefined (potentially infinite), we address this challenge by creating a mask. This mask is employed to conceal nodes corresponding to these specific variants/country pairs, ensuring they do not contribute to our training loss. Essentially, our graph models are not trained on these nodes.

2) *Emergence Prediction*: For the problem of emergence prediction, the chosen loss function is the Binary Cross Entropy (BCE) Loss. In addition to this, we note that when a new variant appears, it only reaches a maximum of 38 countries out of the 87, resulting in a large class imbalance. To account for the class imbalances, class weights are applied to the loss function, providing a balanced learning approach. These weights were calculated using the Inverse Class Frequency method [42].

#### IV. EXPERIMENTS

##### A. Dataset

To validate our methodology, we've used a combination of multiple datasets which are detailed below.

1) *Covariant Data*: CoVariants [12] is our primary dataset which provides the current state of variants and mutations of interest for SARS-CoV-2. This data is enabled by GISAID [43] and ranges from August 2020 through October 2023, with a bi-weekly resolution for 36 variants starting from 20A.EU1 to 23F.Omicron, which is current as of this work. CoVariants follows the NextStrain Clade schema [44], in which variants can descend from other variants.

2) *Border Restrictions Data*: We considered the border restrictions data provided in the OxCGRT [39] dataset, with details on what level of border controls were enacted by governments in real-time from Jan 1, 2020, to Jan 8, 2023. OxCGRT measured the variations in government responses using their COVID-19 Government Response Stringency Index, which is a simple additive score of nine indicators ranging from school closures to vaccination policies. Of these indicators, we picked international travel closure controls since they best represent

the goal of this paper in capturing the emergence and cross-border transmission of variants. These values are encoded in an ordinal scale as follows: 0 - no measures, 1 - screening, 2 - quarantine on high risk region, 3 - ban on high risk regions, 4 - total border closure. The recorded values were then scaled down to a range between 0.1 and 1, with 1 indicating no border restrictions and 0.1 representing complete border closure. Note that 0.1 was chosen over 0, acknowledging the possibility of some mobility between connecting countries due to necessary trade or border crossings via open land routes. Furthermore, given that our CoVariants data extends beyond January 2023, we extend OxCGRT by making the assumption that all border restrictions have remained unchanged since Jan 8, 2023.

3) *Country Graphs*: We considered two graphs representing the interconnection between countries. This dataset depicts country neighborhoods according to the Correlates of War (CoW) database. Countries were also deemed neighbors if they share a land or river border or are located within 24 miles of each other across bodies of water. **Adjacency**: We used the country adjacency dataset [45], which offers a list of countries and their neighboring countries. **OpenFlights**: This is a collection of regular flights along with their routes mapped from airports around the world [46]. Given the scope of the current work, we primarily focus on airports and the flight route data, and was mainly used during ablation studies. Airports data is a UTF-8 encoded collection of over 14,000 airports, train stations and ferry terminals across the world as of January 2017. It consists of information like city/country, IATA codes, geographic coordinates and the type of the airport (air terminal, ferry station, etc.). Routes data provides information about 67663 directional routes between 3321 airports on 548 airlines. This dataset was used in an ablation study to validate the effectiveness of utilizing these flight routes as edges in our graph creation process.

##### B. Benchmark Pipeline

As previously mentioned, we are the first to attempt this type of problem as far as we know. In Figure 5, we present the comprehensive pipeline employed for the retrospective

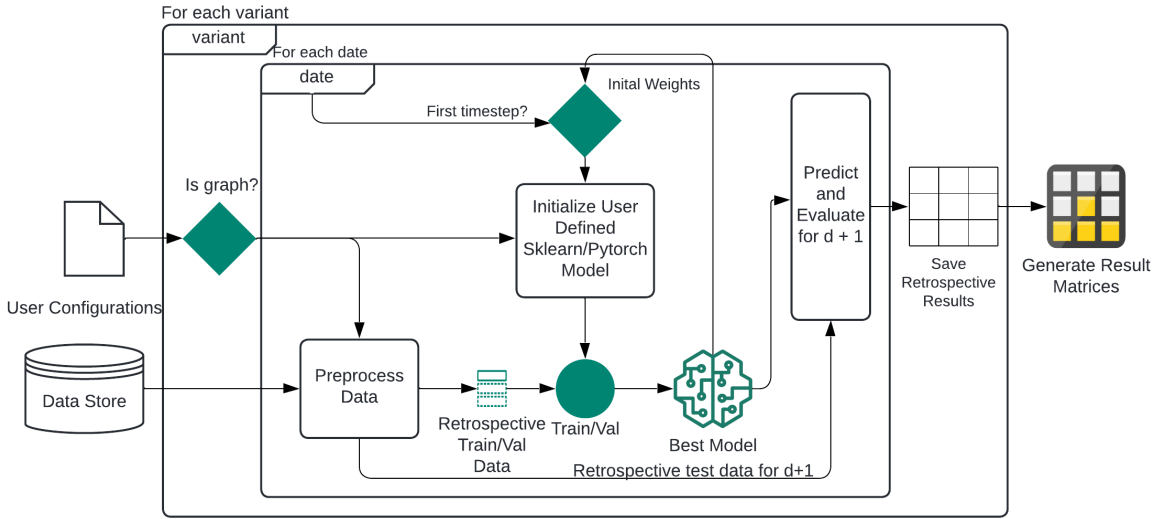


Fig. 5: Benchmarking Pipeline

training, validation, and testing of diverse models. The design of this pipeline prioritizes user-friendliness, allowing seamless integration of new PyTorch models or direct utilization of scikit-learn models through a configuration file. Users only need to specify whether the model requires the use of graph data and the nature of the task, whether it involves Delay Prediction or Emergence Prediction, leaving the pipeline to handle the rest. Additionally, the data pre-processing is encapsulated in a separate function, providing users with the flexibility to make any necessary modifications. This approach facilitated the training of various benchmark models on our dataset and extends an accessible framework for users to experiment with their own models.

As shown in Figure 5, the evaluation is also being done retrospectively. It means that for each date that the model is trained on, it is used to predict for the subsequent date representing a 1-timestep ahead forecast. This aligns with the biweekly nature of the data, resulting in a two-week ahead forecast. Furthermore, model performance is being evaluated per variant, meaning that for each given variant we retrospectively assess the trained models over time.

In the context of delay prediction, considering the biweekly data, the target is consistently a multiple of 14 days. Therefore, the output of our models is always rounded up to the nearest multiple of 14. Furthermore, evaluations exclude countries where a variant has already become dominant or never achieves dominance. To measure performance, we define Mean/Median Absolute Errors (MAE/MedAE) as follows:

$$\text{MAE}_{t,v} = \frac{1}{N_s} \sum_{i=1}^{N_s} |\hat{y}_{i,t,v} - y_{i,t,v}| \quad (17)$$

$$\text{MedAE}_{t,v} = \text{median}(|\hat{y}_{i,t,v} - y_{i,t,v}|) \quad (18)$$

where  $i$  ranges from 1 to  $N_s$  and  $N_s$  represents the number of valid countries to predict for. The  $t, v$  subscripts indicate that these errors are calculated for each variant at each

timestep. Since this problem is retrospective, we also evaluate performance over time by finding the mean and median of the errors:

$$\text{MMAE}_v = \frac{1}{T} \sum_{t=1}^T (\text{MAE}_{v,t})$$

$$\text{MMedAE}_v = \frac{1}{T} \sum_{t=1}^T (\text{MedAE}_{v,t})$$

$$\text{MedMAE}_v = \text{median}(\text{MAE}_{v,t})$$

$$\text{MedMedAE}_v = \text{median}(\text{MedAE}_{v,t})$$

where  $t$  ranges from 1 to  $T$  and  $T$  represents the total number of timesteps for which the variant  $v$  circulates before reaching total dominance, i.e. it globally reached all its targets and begins to disappear. Finally, we conduct a mean across all the variants  $v$  to get our four error metrics: MMAE, MMedAE, MedMAE, and MedMedAE. While all these metrics offer valuable insights, our main focus lies on MedMAE and MedMedAE, emphasizing median performance over time. This choice is made due to certain data inconsistencies, such as variants appearing in a single country for an extended period before spreading to other countries, resulting in large errors that may skew results.

In the context of emergence prediction, our objective is to retrospectively predict whether a given variant will become dominant in each country. Given the presence of class imbalance in our data, we employ the Macro F1-score as an evaluation metric, which considers both precision and recall across all classes, providing a balanced assessment [47], [48].

### C. Pre-processing

The initial pre-processing stage focused on aligning the country names across diverse datasets, with an emphasis on inclusion based on data availability. Only countries present in all datasets were retained, ensuring a standardized set for

subsequent analyses. A specific adjustment was necessary for the OpenFlights dataset, involving the mapping of city routes to their respective country routes. Leveraging the provided airport data, which contains comprehensive city and country details, facilitated this mapping process. The transformation ensured that subsequent analyses operated consistently at the country level.

For each country, the prevalence of each variant, defined in equation 1, was calculated at each timestep. Variants with a prevalence of less than 5% were disregarded in our analysis. To calculate the prevalence ratios, the two variants with the highest prevalence were identified for each timestep. For each variant on that particular day, the prevalence ratio was calculated using equation 2. Finally, variants that did not reach a prevalence ratio of 0.2 or those that were present in less than three countries were filtered out. These steps ensured that only variants with a significant presence and wide geographic distribution were included in the subsequent analysis. All subsequent pre-processing steps were conducted retrospectively. This implies that as time progresses, more data is used for computing the global growth rates ( $S$ ) and more data is available for training. Notably, for our dynamics-based model, this retrospective process also involved interpolating biweekly data into a daily resolution using a cubic smoothing spline. This adjustment was deemed necessary due to the transient nature of variants. The biweekly data has a resolution that is too coarse to adequately capture the linear relationships between the delay in variant transmission from one country to another and its prevalence in the latter.

#### D. Benchmark Models

We implemented a number of benchmark models that act as baselines for comparisons.

**Mean Model – Delay Prediction:** This model predicts delays based on average delays on the variants between the countries under consideration. Specifically, at time  $t$ , for a new variant  $i$  on a target country  $p$ , suppose  $Q$  is the set of all countries where the variant has appeared in. Then, the predicted time of arrival is given by

$$t_i^p = t + \text{median}_q (\text{mean}_j (\Delta_j(p, q))) . \quad (19)$$

Here  $\Delta_j(p, q)$  is the delay between the appearance of variant  $j$  from country  $q$  to country  $p$ . We take the mean of  $\Delta_j(p, q)$  over all prior variants  $j$  that appeared in both countries  $p$  and  $q$ . Finally, we take the median of the delays over all countries in  $Q$  where variant  $i$  has already appeared.

**Trivial Model – Emergence Prediction:** This model sets all predictions to 1. In other words, this model consistently predicts that a variant will emerge in all countries

**Dynamics-based Model – Delay Prediction:** This is the dynamics-based linear model discussed in Section III-C. This model serves as a baseline mechanistic model, which, under the right assumptions, offers an explainable and efficient method for calculating delays.

**Adjacency-based Model – Emergence Prediction:** We use a simple adjacency-based classifier. At a given timestep,  $\tau$ , and

variant,  $v$ , we check all countries in which  $v$  is dominant. If it is dominant in a country  $c$ , we predict that the variant  $v$  will become dominant in all countries adjacent to  $c$  at  $\tau + 1$ .

**Decision Tree:** We use Decision Tree classifiers and regression models to address Emergence Prediction and Delay Prediction, respectively. As discussed in Section IV-B, this involves transforming the dataset into an  $N \times 5$  matrix. Here,  $N$  represents the total number of samples, where each sample corresponds to the 5 features of a given variant at a specific point in time in a specific country. These trees use the Gini impurity and mean squared error for their criterion functions. No maximum depth was set for either.

**Multi Layer Perceptron:** We employ a Multi-Layer Perceptron (MLP) classifier and regressor for Emergence Prediction and Delay Prediction, respectively. They were configured with two hidden layers, consisting of 16 and 8 neurons, respectively. The selection of hyperparameters, including the number of hidden layers, activation function, and solver, was determined through comprehensive experimentation and optimization tailored to our specific problem. The training procedure closely followed the approach outlined in Section III-E, with the only distinction being the structuring of our dataset into an  $N \times 5$  matrix, as described previously. A batch size equivalent to the number of countries was used, where each batch represented the list of countries and their features at each timestep for each variant, ensuring that the gradient updates were performed collectively for each group.

**Gated Recurrent Unit Network** We utilize a simple GRU network to encode the temporal information of variant transmissions and predict their emergence and delay. To train this model, first, we feed temporal features of the variant to the GRU architecture which embeds them for each country distinctly. Then, we flatten the embedded features and append them with  $S$  and directly give them to an FC layer for predicting the time it takes for that variant to appear in a specific country. We employ GraphNorm layer here after the concatenation to accelerate training by smoothing graph aggregation distributions.

**Graph Convolutional Network (GCN)** We consider a simple GCN, with a basic architecture in an attempt to capture local relationships and features within the graph structure. It is comprised of two GCN layers, which output 32 and 16 channels respectively. Dropout is strategically employed between these two layers for regularization. The final graph embedding is flattened and fed into an FC layer which outputs the delay or emergence for each country.

**Encoded Dynamics GCN** Since each country possesses a variable number of circulating variants with different growth rates  $S$  (as derived in III-B), we can learn a latent vector representation  $Z$  of this data through the use of encoders. We achieve this in two ways:

**Using an Autoencoder (AE-GCN):** We employ a simple autoencoder with two linear layers and ReLU activation in the encoder and decoder blocks.

The model takes a variable-sized input  $S_{pt}$ , a subset of variants (retrospective) in a region  $p$  at a given time instance

TABLE I: Emergence Prediction f1-scores

Model	f1
Trivial Model	0.20
Adjacency-based Model	0.58
<b>Decision Tree</b>	<b>0.96</b>
MLP	0.93
<b>GRU</b>	<b>0.96</b>
GCN	0.73
T-GCN	0.77
AE-GCN	0.73
EE-GCN	0.74

TABLE II: Delay Prediction Errors

Model	MedMedAE	MedMAE
Mean Model	21.18	26.73
<b>Dynamics-based Model</b>	<b>17.25</b>	34.1
Decision Tree	22.91	23.63
MLP	24.98	23.91
GRU	20.85	22.85
GCN	19.09	21.73
<b>T-GCN</b>	<b>18.45</b>	<b>19.08</b>
AE-GCN	19.77	22.77
EE-GCN	21.00	24.46
DIL-GCN	20.33	22.71

*t*. We train the autoencoder using MSE loss. We append the learned encoding from this training process to the feature matrix before constructing a spatio-temporal snapshot graph data for the GCN model (defined earlier).

**Embedded Encoder (EE-GCN):** Using an autoencoder implies that the model is guided towards learning an embedding using the decoder output, and these two are inherently separate models. The encoder weights are also unaffected during graph training. An alternative approach is to embed this into the larger GCN model. In this method, as before, the variable-sized  $S_{pt}$  is fed to an encoder block (consisting of two linear layers with ReLU activation). Instead of using a decoder, we directly concatenate the resulting latent vector representation  $Z$  to the node features fed into the GCN. This means the encoder weights are updated in the graph training loop, allowing the model to learn a better latent representation.

## E. Results

1) *Emergence Prediction:* Table I shows the macro F1-scores for emergence prediction across different models. Notably, the Decision Tree and GRU models exhibit high F1-scores, outperforming all other models. While the T-GCN achieves a reasonable performance here relative to the adjacency-based and trivial models, it does not come close to competing with the simpler ML-based models or the GRU. This suggests that identifying the emergence of a variant can be more straightforward and often involves distinct, separable patterns that decision trees and GRUs can efficiently learn.

2) *Delay Prediction:* Table II presents the performance metrics for delay prediction across the various models. The evaluated metrics include MedMedAE and MedMAE, as discussed in Section IV-B. The results indicate that the dynamics-based model, employing a dynamics-based linear approach, outperforms all other models in terms of MedMedAE, with T-GCN performing the next best. Additionally, the proposed T-

GCN achieves the best MedMAE, showcasing its effectiveness in capturing temporal dependencies for delay prediction, while the dynamics-based model performs worse than all other models in this metric. This suggests that the dynamics-based model is susceptible to outlier predictions for some country pairs, which skews its results. Additionally, we observe that the DIL-GCN does not surpass its GCN counterpart, highlighting the unnecessary use of dynamics as a regularization of the loss when employing the correct features.

## V. DISCUSSION

In this section, we conduct a detailed examination of our results, show the effectiveness of integrating variant dynamics into our models, and provide justification for the construction of our graph. Note that since high performance was achieved for emergence prediction, this analysis will primarily focus on delay prediction.

### A. Results Analysis

Figure 6 provides a detailed representation of the results for the dynamics-based model and T-GCN model. The heatmaps illustrate the number of countries eligible for predicting at each timestamp. The numbers indicate the errors over time for each variant throughout their existence. Some variants exhibit NaN values for the dynamics-based model. This occurs due to two primary reasons. Firstly, the linear model requires a minimum of two common variants between two countries to build an effective model. Secondly, the linear model can encounter significant challenges when variant  $j$  is identical in growth rate to variant  $k$  (i.e.,  $S_j = S_k$ ). In such cases, the linear model fits a plane solely along  $Z_1 = 0$  as seen in Equation 14. When variant  $j$  is no longer identical to variant  $k$  for another variant, this model fails drastically, as  $Z_1 \neq 0$ . These scenarios were more prevalent in the early stages of the pandemic when only a few variants were circulating, leading to their exclusion from the dynamics-based model's training process. All final errors, for all models in Section IV-D, were calculated excluding these variants to ensure a fair comparison between the models.

The observations from Figure 6a give us two key insights. Firstly, the primary source of error is associated with variants that persist for an extended duration, such as 21J.Delta or 23E.Omicron. Examining the color gradients, these variants appear to linger in only a few countries before spreading to others. In reality, variants typically do not endure for such prolonged periods without either being superseded by another variant or transmitting to additional countries [38], [49]. This suggests a potential issue in the data capturing these lingering variants. Secondly, despite this being a major source of error for GCN-based models, they exhibit overall robustness to outlier predictions, unlike the dynamics-based model as seen in Figure 6b. Also, note that our ground truth is at a granularity of 14 days which may inflate the error. Suppose, in reality, the first day of a variant reaching a desired prevalence threshold is  $t = 14k + 1$ , for some integer  $k$ . In the ground truth, it will appear at the next multiple of 14, i.e.,  $t + 13$ . If our prediction was  $t' = 14k = t - 1$ , the actual error is 1 day, while in

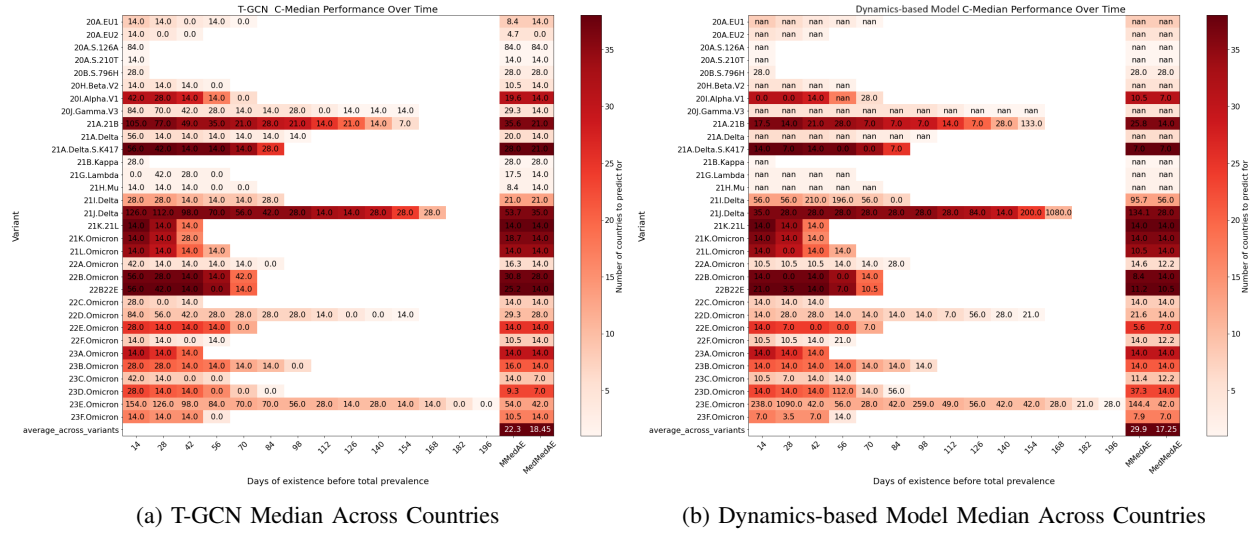


Fig. 6: Results matrices for the best-performing delay prediction models. The heatmaps display both the errors and the number of countries being predicted for at each timestep until they are no longer dominant anywhere. This is important for analysis as variants may not reach all countries.

comparison to the observed ground truth, it will result in an error of 14 days.

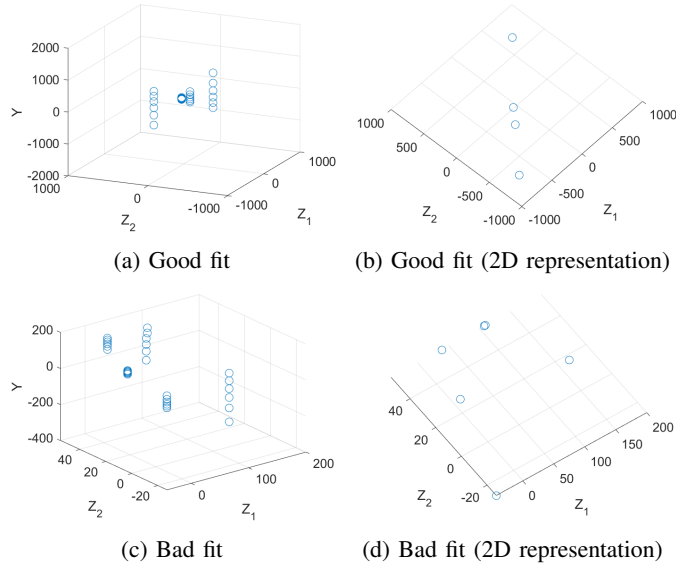


Fig. 7: 3D plots of the X and Y points in space, from equation 14, and their 2D representations. Examples are taken for two linear models fitting on data for 22A Omicron.

While the dynamics-based model does output very good predictions, it fails often and dramatically in some cases. Figure 7 presents examples of 3D points in space utilized for fitting linear models. In Figure 7a, the 3D points form a space where a plane can be fitted exceptionally well. However, as newer COVID variants emerge, the dynamics may evolve, causing some initial assumptions, such as full cross-

TABLE III: Dynamics Ablations MedMedAE

Model	$[r S]$	$r$	$[p S]$	$p$	$S$
Decision Tree	<b>22.91</b>	27.36	23.39	25.77	23.86
MLP	24.98	26.73	24.34	25.93	<b>23.86</b>
GRU	<b>20.85</b>	21.05	21.05	23.27	n/a
GCN	<b>19.09</b>	21.00	20.68	21.00	20.36
T-GCN	<b>18.45</b>	19.73	22.27	20.36	n/a

immunity [38], to become invalid. This evolution makes it more challenging to perfectly fit a linear model, as depicted in Figure 7c.

### B. Ablation Studies

In this section, we study the effectiveness of our design choices. While MedMedAE was used as our metric of choice, MedMAE also provided similar results here.

1) *Dynamics*: We examine the usefulness of integrating the extracted dynamics as inputs for our models. In this analysis, we train the same models using different sets of features. Specifically, we investigate the effectiveness of using  $S$  as a feature and the impact of using a time series of  $r$ . The feature configuration  $[r|S]$  is detailed in Section III-D1, while  $r$  excludes  $S$  as a feature, relying solely on the time series of prevalence ratios rather than the prevalence  $p$ . Additionally, we further investigate the effectiveness of  $S$  by comparing  $[p|S]$  to  $p$  and the utilization of  $S$  as the only feature.

From the results in table III, we observe that the  $[r|S]$  combination outperformed all other configurations except for the case of the MLP. There is also an improvement when utilizing  $r$  over  $p$  for the temporal-based models, with the GCN performing similarly and the others exhibiting poorer performance. This suggests that the temporal models effectively encode the latent information contained in the time series of  $r$ , while the simpler models struggle to do so. Additionally, the

TABLE IV: Graph Ablation Results

Model	MedMedAE	MedMAE
GCN	<b>19.09</b>	<b>21.73</b>
GCN_30	20.67	23.29
GCN_60	21.64	23.36
GCN_flights_adj	24.82	23.36
GCN_flights	24.18	24.00
GCN_fullcon	26.09	25.29
GCN_WoEW	20.68	23.34

inclusion of  $S$  as a feature enhances results across all cases. Even when used in isolation,  $S$  performs generally better than the models relying solely on a time series. Combining  $S$  and  $r$  significantly improves performance in most cases, indicating a synergistic effect likely stemming from the linear relationship between the two, as discussed in Section III-D1. It is important to note that the GRU and T-GCN were not trained using just  $S$  since excluding the time series encoding reduces these models to a MLP and GCN, respectively.

2) *Graphs*: When designing the structure of our graph, several considerations were taken. Firstly, we acknowledged that certain nodes (countries) might be more susceptible to noise due to reporting inconsistencies or a lack of reporting, leading to unreliable data. To address this issue, we explored the option of using only countries with consistently reported data, focusing on the top 30 (GCN\_30) and top 60 (GCN\_60) countries out of the total 87 (GCN) countries in our dataset. Additionally, we examined different approaches for creating edges in our graph. While country adjacency served as the base (GCN), we also explored the option of connecting countries through flight routes using the OpenFlights dataset. This exploration included a combination of country adjacency and flight routes (GCN\_flights\_adj), as well as utilizing only flight routes (GCN\_flights). We also include a fully connected graph (GCN\_fullcon) for comparison. All these graphs incorporated dynamic weights for their edges, with the exception of GCN\_WoEW, which was utilized as a comparison. These ablations were conducted using a simple two-layer GCN to isolate and understand the impact of individual components or features on the overall model performance.

From Table IV, it is evident that our selected graph design, based on country adjacency, outperforms alternative configurations. The number of nodes (countries) in the graph does not significantly impact the model performance. In contrast, an FC graph performs the worst, underscoring the importance of considering specific relationships between countries rather than creating direct connections between all nodes. Interestingly, the use of flight routes generally results in increased errors. While this might seem counter-intuitive, considering that flights could connect continents, it's crucial to note that, based on the definition of country adjacency in Section IV-A, countries like the USA and Russia are considered adjacent. As a result, they act as a link between continents. Additionally, the inclusion of dynamic weights in the edges proves beneficial for the overall model performance.

3) *Dominance*: We established our dominance threshold, denoted as  $\theta$ , with a value of  $\frac{1}{3}$  in Section III-A. The impact of

TABLE V: Threshold Ablation Results for GCN

$\theta$	MedMedAE	MedMAE	f1
$\frac{1}{9}$	33.41	37.81	0.77
$\frac{1}{4}$	20.68	24.30	0.75
$\frac{1}{3}$	19.09	21.73	0.73
$\frac{1}{2}$	18.45	20.88	0.76
1	17.5	21.56	0.73

varying  $\theta$  is presented in Table V. While this variation does not significantly influence the problem of emergence prediction, it does play a role in delay prediction. We observe that increasing values of  $\theta$  corresponds to decreasing errors. This phenomenon is likely attributed to the fact that the arrival of a variant heavily depends on its status in neighboring countries. Once a variant arrives, its potential to achieve dominance or not simply hinges on its behavior in other countries. This explains why emergence prediction is less affected. However, delay prediction is more complex. Following a variant's arrival in a country, its trajectory to higher prevalence is largely influenced by internal factors such as the mobility within the country and the precautionary measures implemented by the government to impede its spread. A larger threshold provides the model with more time to leverage these internal dynamics, resulting in more accurate predictions for delay.

### C. Implementation

The main pipeline depicted in Figure 5, was implemented in Python. The dynamics-based model and dynamics-based delay prediction models were implemented using MATLAB, following a similar overall pipeline. The implementation was carried out on a machine equipped with a 32-core Intel(R) Xeon(R) Gold 5218 CPU running at 2.3 GHz and 64 GB of RAM. Focusing on the example of variant 23F.Omicron at a single timestep, which contains the majority of the data, and the heaviest model (T-GCN), the average runtimes for different components were approximately 32s for data pre-processing, 20s for training, and 0.01 seconds for inference. The entire retrospective pipeline takes approximately 2 hours to complete. Notably, the most time-consuming aspect of the retrospective pipeline is the data pre-processing step, which could potentially be optimized further through memoization.

## VI. CONCLUSION

We addressed the challenges of predicting variant emergence and delay across countries. The derivation of variant dynamics provided a theoretical foundation, which was used to engineer relevant features as well as a novel dynamics-based model. We demonstrated that our dynamics-informed GNN approach outperformed all other methods. Through comprehensive experiments and analysis, we demonstrated the effectiveness of our design choices, providing valuable tools for understanding and predicting the intricate relationships and connectivity patterns between nations. Furthermore, as we are the first to address the proposed problem, we provided a comprehensive benchmark and make our full pipeline available in an effort to facilitate research in the field.

## REFERENCES

- [1] “World health organization covid-19 dashboard,” 2023.
- [2] T. L. Wiemken, F. Khan, L. Puzniak, W. Yang, J. Simmering, P. Polgreen, J. L. Nguyen, L. Jodar, and J. M. McLaughlin, “Seasonal trends in covid-19 cases, hospitalizations, and mortality in the united states and europe,” *Scientific Reports*, vol. 13, Mar. 2023.
- [3] “Tracking sars-cov-2 variants,” 2023.
- [4] P. V. Markov, M. Ghafari, M. Beer, K. Lythgoe, P. Simmonds, N. I. Stilianakis, and A. Katzourakis, “The evolution of sars-cov-2,” *Nature Reviews Microbiology*, vol. 21, p. 361–379, Apr. 2023.
- [5] A. S. Lambrou, P. Shirk, M. K. Steele, P. Paul, C. R. Paden, B. Cadwell, H. E. Reese, Y. Aoki, N. Hassell, X.-Y. Zheng, *et al.*, “Genomic surveillance for sars-cov-2 variants: predominance of the delta (b. 1.617. 2) and omicron (b. 1.1. 529) variants—united states, june 2021–january 2022,” *Morbidity and Mortality Weekly Report*, vol. 71, no. 6, p. 206, 2022.
- [6] J. Sun, X. Chen, Z. Zhang, S. Lai, B. Zhao, H. Liu, S. Wang, W. Huan, R. Zhao, M. T. A. Ng, *et al.*, “Forecasting the long-term trend of covid-19 epidemic using a dynamic model,” *Scientific reports*, vol. 10, no. 1, p. 21122, 2020.
- [7] H. Hu, H. Du, J. Li, Y. Wang, X. Wu, C. Wang, Y. Zhang, G. Zhang, Y. Zhao, W. Kang, *et al.*, “Early prediction and identification for severe patients during the pandemic of covid-19: a severe covid-19 risk model constructed by multivariate logistic regression analysis,” *Journal of Global Health*, vol. 10, no. 2, 2020.
- [8] J. T. Wu, K. Leung, and G. M. Leung, “Nowcasting and forecasting the potential domestic and international spread of the 2019-ncov outbreak originating in wuhan, china: a modelling study,” *The lancet*, vol. 395, no. 10225, pp. 689–697, 2020.
- [9] D. A. Shah, E. D. De Wolf, P. A. Paul, and L. V. Madden, “Accuracy in the prediction of disease epidemics when ensembling simple but highly correlated models,” *PLOS Computational Biology*, vol. 17, pp. 1–23, 03 2021.
- [10] S. Palaniappan, R. V. and B. David, “Prediction of epidemic disease dynamics on the infection risk using machine learning algorithms,” *SN computer science*, vol. 3, no. 1, p. 47, 2022.
- [11] M. Raissi, P. Perdikaris, and G. E. Karniadakis, “Physics-informed neural networks: A deep learning framework for solving forward and inverse problems involving nonlinear partial differential equations,” *Journal of Computational Physics*, vol. 378, pp. 686–707, 2019.
- [12] E. B. Hodcroft, “Covariants: Sars-cov-2 mutations and variants of interest,” 2021.
- [13] “Cdc variant classifications.” <https://www.cdc.gov/coronavirus/2019-ncov/variants/variant-classifications.html>, 2023. Centers for Disease Control and Prevention.
- [14] L. J. Beesley, K. R. Moran, K. Wagh, L. A. Castro, J. Theiler, H. Yoon, W. Fischer, N. W. Hengartner, B. Korber, and S. Y. Del Valle, “Sars-cov-2 variant transition dynamics are associated with vaccination rates, number of co-circulating variants, and convalescent immunity,” *eBioMedicine*, vol. 91, p. 104534, May 2023.
- [15] “Covid 19 forecast hub us.”
- [16] K. Sherratt, H. Gruson, R. Grah, H. Johnson, R. Niehus, B. Prasse, F. Sandmann, J. Deuschel, D. Wolfram, S. Abbott, and *et al.*, “Predictive performance of multi-model ensemble forecasts of covid-19 across european nations,” Apr 2023.
- [17] “The german and polish covid-19 forecasthub.”
- [18] F. Scarselli, M. Gori, A. C. Tsoi, M. Hagenbuchner, and G. Monfardini, “The graph neural network model,” *IEEE transactions on neural networks*, vol. 20, no. 1, pp. 61–80, 2008.
- [19] M. Raissi, P. Perdikaris, and G. E. Karniadakis, “Physics-informed neural networks: A deep learning framework for solving forward and inverse problems involving nonlinear partial differential equations,” *Journal of Computational physics*, vol. 378, pp. 686–707, 2019.
- [20] S. Nagpal, R. Pal, Ashima, A. Tyagi, S. Tripathi, A. Nagori, S. Ahmad, H. P. Mishra, R. Malhotra, R. Kutum, and T. Sethi, “Genomic surveillance of COVID-19 variants with language models and machine learning,” *Frontiers in Genetics*, vol. 13, Apr. 2022.
- [21] S. Basu and R. H. Campbell, “Classifying COVID-19 variants based on genetic sequences using deep learning models,” June 2021.
- [22] E. Kharazmi, M. Cai, X. Zheng, Z. Zhang, G. Lin, and G. E. Karniadakis, “Identifiability and predictability of integer and fractional-order epidemiological models using physics-informed neural networks,” *Nature Computational Science*, vol. 1, no. 11, pp. 744–753, 2021.
- [23] I. Kiselev, I. Akberdin, and F. Kolpakov, “Delay-differential seir modeling for improved modelling of infection dynamics,” *Scientific Reports*, vol. 13, no. 1, p. 13439, 2023.
- [24] A. Rodríguez, J. Cui, N. Ramakrishnan, B. Adhikari, and B. A. Prakash, “Einns: Epidemiologically-informed neural networks,” in *Proceedings of the AAAI Conference on Artificial Intelligence*, vol. 37, pp. 14453–14460, 2023.
- [25] X. Ning, L. Jia, Y. Wei, X.-A. Li, and F. Chen, “Epi-dnns: Epidemiological priors informed deep neural networks for modeling covid-19 dynamics,” *Computers in biology and medicine*, vol. 158, p. 106693, 2023.
- [26] M. R. Davahli, K. Fiok, W. Karwowski, A. M. Aljuaid, and R. Taiar, “Predicting the dynamics of the covid-19 pandemic in the united states using graph theory-based neural networks,” *International Journal of Environmental Research and Public Health*, vol. 18, p. 3834, Apr 2021.
- [27] J. Gao, R. Sharma, C. Qian, L. M. Glass, J. Spaeder, J. Romberg, J. Sun, and C. Xiao, “STAN: spatio-temporal attention network for pandemic prediction using real-world evidence,” *Journal of the American Medical Informatics Association*, vol. 28, pp. 733–743, 01 2021.
- [28] G. Panagopoulos, G. Nikolentzos, and M. Vazirgiannis, “Transfer graph neural networks for pandemic forecasting,” 2021.
- [29] I. Sung, S. Lee, M. Pak, Y. Shin, and S. Kim, “AutoCoV: tracking the early spread of COVID-19 in terms of the spatial and temporal patterns from embedding space by k-mer based deep learning,” *BMC Bioinformatics*, vol. 23, Mar. 2022.
- [30] S. Ganesan and D. Subramani, “Spatio-temporal predictive modeling framework for infectious disease spread,” *Scientific Reports*, vol. 11, no. 1, p. 6741, 2021.
- [31] S. Seo, C. Meng, and Y. Liu, “Physics-aware difference graph networks for sparsely-observed dynamics,” in *International Conference on Learning Representations*, 2019.
- [32] S. Seo and Y. Liu, “Differentiable physics-informed graph networks,” *arXiv preprint arXiv:1902.02950*, 2019.
- [33] A. Chopra, A. Rodríguez, J. Subramanian, A. Quera-Bofarull, B. Krishnamurthy, B. A. Prakash, and R. Raskar, “Differentiable agent-based epidemiology,” *arXiv preprint arXiv:2207.09714*, 2022.
- [34] A. Chopra, E. Gel, J. Subramanian, B. Krishnamurthy, S. Romero-Brufau, K. S. Pasupathy, T. C. Kingsley, and R. Raskar, “Deepabm: scalable, efficient and differentiable agent-based simulations via graph neural networks,” *arXiv preprint arXiv:2110.04421*, 2021.
- [35] S. Deng, S. Wang, H. Rangwala, L. Wang, and Y. Ning, “Graph message passing with cross-location attentions for long-term ili prediction,” *arXiv preprint arXiv:1912.10202*, 2019.
- [36] A. Kapoor, X. Ben, L. Liu, B. Perozzi, M. Barnes, M. Blais, and S. O’Banion, “Examining covid-19 forecasting using spatio-temporal graph neural networks,” *arXiv preprint arXiv:2007.03113*, 2020.
- [37] A. Srivastava, “The variations of sikjalpa model for covid-19 forecasting and scenario projections,” *Epidemics*, vol. 45, p. 100729, 2023.
- [38] J. Chen, C. Gu, Z. Ruan, and M. Tang, “Competition of sars-cov-2 variants on the pandemic transmission dynamics,” *Chaos, Solitons; Fractals*, vol. 169, p. 113193, Apr. 2023.
- [39] T. Hale, N. Angrist, R. Goldszmidt, B. Kira, A. Petherick, T. Phillips, S. Webster, E. Cameron-Blake, L. Hallas, S. Majumdar, *et al.*, “A global panel database of pandemic policies (oxford covid-19 government response tracker),” *Nature human behaviour*, vol. 5, no. 4, pp. 529–538, 2021.
- [40] K. Cho, B. Van Merriënboer, C. Gulcehre, D. Bahdanau, F. Bougares, H. Schwenk, and Y. Bengio, “Learning phrase representations using rnn encoder-decoder for statistical machine translation,” *arXiv preprint arXiv:1406.1078*, 2014.
- [41] T. Cai, S. Luo, K. Xu, D. He, T.-Y. Liu, and L. Wang, “Graphnorm: A principled approach to accelerating graph neural network training,” 2021.
- [42] Y. Cui, M. Jia, T.-Y. Lin, Y. Song, and S. Longie, “Class-balanced loss based on effective number of samples,” 2019.
- [43] S. Khare, C. Gurry, L. Freitas, M. B. Schultz, G. Bach, A. Diallo, N. Akite, J. Ho, R. T. Lee, W. Yeo, G. C. C. Team, and S. Maurer-Stroh, “Gisaid’s role in pandemic response,” *China CDC Weekly*, vol. 3, p. 1049, 2021.
- [44] I. Aksamentov, C. Roemer, E. B. Hodcroft, and R. A. Neher, “Nextclade: clade assignment, mutation calling and quality control for viral genomes,” *Journal of Open Source Software*, vol. 6, no. 67, p. 3773, 2021.
- [45] Plsec, “Country adjacency,” 2013.

- [46] OpenFlights, “OpenFlights dataset.” <https://openflights.org/>, 2023. Accessed: August 10, 2023.
- [47] J. Opitz and S. Burst, “Macro f1 and macro f1,” *arXiv preprint arXiv:1911.03347*, 2019.
- [48] Z. C. Lipton, C. Elkan, and B. Naryanaswamy, “Optimal thresholding of classifiers to maximize f1 measure,” in *Machine Learning and Knowledge Discovery in Databases: European Conference, ECML PKDD 2014, Nancy, France, September 15-19, 2014. Proceedings, Part II 14*, pp. 225–239, Springer, 2014.
- [49] “A timeline of covid-19 variants,” 2023.